MULTI-STAGE AND SPARSE EQUALIZER DESIGN FOR COMMUNICATION SYSTEMS IN REVERBERANT UNDERWATER CHANNELS

Karl F. Nieman, Kenneth A. Perrine, Keith H. Lent, Terry L. Henderson, Terry J. Brudner and Brian L. Evans

Advanced Technology Laboratory, Applied Research Laboratories
The University of Texas at Austin, Austin, TX

{nieman, perrine, lent, henderson, brudner}@arlut.utexas.edu and bevans@ece.utexas.edu

ABSTRACT

Coherent underwater communication systems in shallow water must compensate for several impairments, including Doppler shift and reverberant channels. In this paper, we quantify tradeoffs in communication performance vs. computational complexity in designing receivers to compensate for these impairments. Our communication system is unidirectional, single-carrier, wideband, and packet-based. We use 1.5 hours of recorded data from an experimental system on a public lake with a moving transmitter and stationary receiver. Our contributions include acoustic channel modeling and a tradeoff analysis for Doppler shift estimation, multi-stage equalizers and sparse equalizers. We compare multi-stage and sparse equalizers against traditional equalizers.

Index Terms— adaptive equalizers, Doppler estimation, reverberant channels, sparse equalizers, underwater acoustic communication

1. INTRODUCTION

Underwater acoustic (UWA) communication channels are generally lowpass channels, with long transmission delays due to acoustic propagation speeds [1][2]. Within a modest range (~500 m), the shallow UWA channel faces significant Doppler distortion, multiple propagation paths, long channel memory, rapid channel fluctuations, and interfering sources. Doppler distortion, or stretching of acoustic waveforms, is caused by both velocity differences between transmitter and receiver, and multipath reflections from moving surfaces.

A modest range, shallow UWA channel has an impulse response with a high amplitude direct path (if the receiver is close enough) followed by time-varying reverberant echoes, as shown in Fig. 1. The impulse response shown represents less than 30% of the total response energy, which can span up to 0.5s after arrival of the direct path. We evaluate equalizers to reduce reverberant interference in a mobile point-to-point communication system. Adaptive equalizers can track and compensate slowly varying Doppler effects.

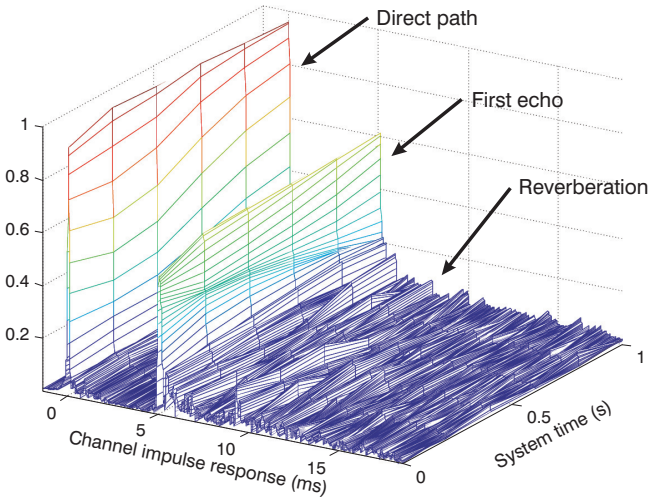

Fig. 1. Channel impulse response magnitude variation vs. time from a boat to a stationary platform at 820 ft (250 m) range. The direct path and first echo are approx. stationary over the system time whereas the reverberation varies largely over the system time.

In this paper, we design receivers for a unidirectional, single-carrier, wideband, packet-based UWA communication system. The system supports three different digital modulation methods at three different carrier frequencies. We evaluate design tradeoffs using 1.5 hours of recorded data from an experimental system on a local public lake with a moving transmitter and a stationary receiver. We analyze design tradeoffs for (1) Doppler shift estimation, (2) multi-stage equalizers and (3) sparse equalizers.

2. BACKGROUND

Our experiments were performed on July 6, 2009, at the Lake Travis Test Station operated by the Applied Research Laboratories at The University of Texas at Austin. This facility is located about 20 miles (30 km) northwest of downtown Austin, Texas. The downstream portion of the lake is contained by a dam, as shown in Fig. 2. The lake continues upstream to follow its former river bed and has a

surface area of 1862 acres (7536 hectares) [3]. The max. depth was estimated to be 120 ft (37m) in July 2009 [4].

Characteristics of the lake create significant challenges for underwater communications. First, sound propagation is affected by the lake's vertical temperature gradients. The slower sound speeds observed at cooler temperatures around greater depths generally cause a downward bending for sound propagation. Additionally, thermoclines, or narrow layers of water exhibiting aberrant temperature gradients, can exist in the lake, which increases the complexity of the propagation of sound. Fig. 3 shows a simulated ray tracing of sound propagation paths. Although this simulation does not address important phenomenon such as upper surface scattering or an irregularly shaped lakebed, it does show the challenges inherent in underwater sound transmission. For example, sound transmitted from Point A cannot likely reach the receiver at Point R without reflecting off of the lake surface subject to dynamic distortions caused by surface ripples. Also, sound transmitted from Point B can only reach Point R via a bottom reflection. Fig. 3 uses the sound speed and temperature profile of the lake shown in Fig. 4.

The geography of the test environment also creates challenges. The flat surface of the dam and steep slopes of the lakebed can create reflections that interfere with the direct path. Rocks and other features on the lake bottom can cause unpredictable reflection paths. Although geographic challenges would likely not be as severe in deeper water, such as an ocean, significant multiple sound paths, volume reverberations, and Doppler distortion would still exist [5].

2.1 Equipment

For all tests, we used an omnidirectional piezoelectric transducer to emit a waveform of nominally 0.5 W RMS transmit power. A directional receive hydrophone was mounted on a planar baffle beneath the barge in Fig. 2. The hydrophone has horizontal and vertical beam widths of approximately 120^{o} and was pointed in the general direction of the transducer. The initial tests mounted a transducer 27 ft (8.2 m) below the water surface on a stationary tower in the lake at a distance of 500 ft (152 m) from the barge. Subsequent tests tethered a transducer to a boat. The tether ranged from 5 to 55 ft (1.5 to 16.8 m) in depth, and distance from the boat to the barge for decodable transmissions varied from 260 to 2120 ft (79 to 646 m). The receiving hydrophone sampled acoustic pressure at a rate of 100 kHz.

2.2 Transmitted Waveforms

The structure of each transmission packet is given in Fig. 5. The beginning was a linearly frequency modulated (LFM) sweep [6] ranging from 5 kHz to 45 kHz over 25 ms. The data portion consisted of a series of raised cosine shaped waveforms for each modulation type given in Table 1.

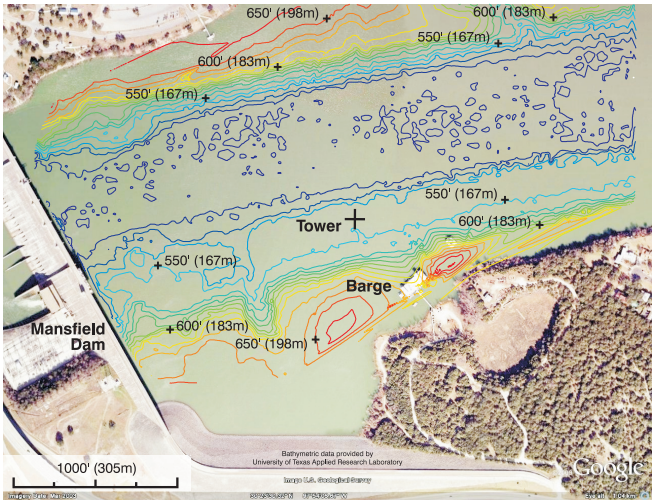

Fig. 2. Aerial view of the Lake Travis test area with a water depth map is shown above. For our tests, the barge was positioned further from the bank than what is depicted in the satellite photo.

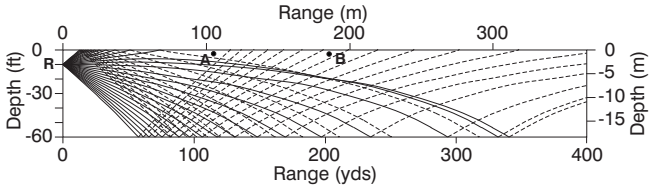

Fig. 3. Simulated sound propagation paths are shown to a receiver R located at a depth of 10 ft (3 m) and range of 0 yds. Sound transmitted from A will likely not reach the receiver R. Although there is no direct path from transmitter B to the receiver R, sound from B reaches R due a reflection off of the bottom.

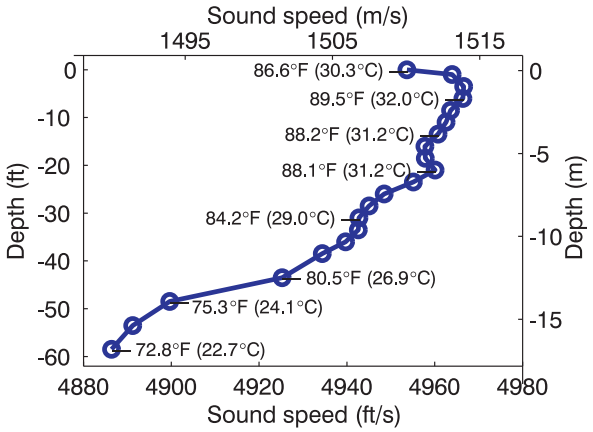

Fig. 4. Sound speeds derived from temperature measurements taken at the time of the experiment on July 6, 2009 at 15:51:00.

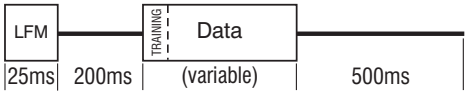

Fig. 5. Temporal layout of one transmission packet is shown. The beginning consists of a linearly frequency modulated (LFM) sweep that ranged from 5 kHz to 45 kHz over 25 ms. The data transmission portion (including training) is given by Table 1.

Table 1. Waveforms for transmitting message data are given below to be used with the packet structure given by Fig. 5. The column labeled α denotes raised-cosine rolloff factor. Later, we will focus our attention on Waveforms 5 and 7 shown in bold.

	Modulation	*Carrier*	*Symbols*	*Sym. Rate*	α
1	BPSK	16.67 kHz	9000	16 kHz	0.04
2	QPSK	16.67 kHz	9000	16 kHz	0.04
3	16-QAM	16.67 kHz	9000	16 kHz	0.04
4	BPSK	25.00 kHz	9000	32 kHz	0.25
5	**QPSK**	**25.00 kHz**	**9000**	**32 kHz**	**0.25**
6	16-QAM	25.00 kHz	9000	32 kHz	0.25
7	**BPSK**	**30.00 kHz**	**900**	**1 kHz**	**1.00**
8	QPSK	30.00 kHz	900	1 kHz	1.00
9	16-QAM	30.00 kHz	900	1 kHz	1.00
10	BPSK	30.00 kHz	9000	9.6 kHz	1.00
11	QPSK	30.00 kHz	9000	9.6 kHz	1.00
12	16-QAM	30.00 kHz	9000	9.6 kHz	1.00

3. SYSTEM MODEL

3.1 Channel Model

Two dominant impairments in the shallow underwater acoustic channel are Doppler effects and reverberation. The received signal $r_i(t)$ through path i from transmitter to receiver can be expressed as a function of time t as

$$r_i(t) = A_i \, f\left((1+d_i)t - \tau_i\right) \tag{1}$$

where A_i is the attenuation due to reflection, absorption loss, and spherical spreading; $f(t)$ is the transmitted signal; d_i is the Doppler shift, expressed as a scaling factor in time; and τ_i is travel time. If N_p paths exist, as encountered in all of our observations, the received signal can be modeled as

$$r(t) = \sum_{i=1}^{N_p} A_i f\left((1+d_i)t - \tau_i\right) + v(t) \tag{2}$$

where $v(t)$ is the additive noise in the channel. We assume that all values of d_i are approx. equal to the bulk Doppler shift d and that d varies slowly over the duration of a packet. Doppler shifts and travel times are in practice independently time-varying, thereby disrupting filter performance if the factor for the dominant path A_i is not suitably greater than the others, and if time variance among paths is significant. Although we find this assumption to be sufficient in many cases, we have also observed cases where no clearly dominant path exists. This is an area of ongoing research.

As shown in Fig. 6, we model the channel according to (2) as a cascade of Doppler distortion that scales the time axis by $\beta = 1 + d$, a long finite impulse response (FIR) filter to model multipath propagation, and additive noise. At 150 m, the observed signal to reverberation floor after Doppler compensation is ~5 dB, whereas observed signal to ambient noise for the widest bandwidth is ~30 dB. At 250 m, the observed signal to reverberation floor after Doppler compensation is ~0 dB, whereas observed signal to ambient noise for the widest bandwidth is ~20 dB.

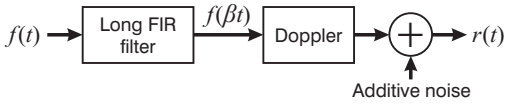

Fig. 6. Channel model uses a finite impulse response (FIR) filter to model multiple propagation paths from transmitter to receiver.

3.2 Receiver Model

Fig. 7 shows the receiver block diagram. Individual data packets are located in time by matched filtering (cross-correlating) the hydrophone data with the transmitted LFM sweeps. The beginning and end of packets are peaks in the matched filtered output that match a set of noise-reducing criteria and are within a window of time that allows for a reasonable range (±0.5%) of Doppler spreading. (Sufficient leeway is given here and in the Doppler shift estimator to accommodate transmissions from moving platforms).

Once a data packet has been detected, it is extracted, basebanded, and downsampled to twice the symbol rate using a polyphase interpolator. The average bulk Doppler shift is then estimated by one of the methods in Section 4.

The real-valued data is then resampled using linear interpolation at a rate adjusted by the average bulk Doppler shift, basebanded, and decimated to twice the symbol rate. In the presence of large Doppler shifts, this pre-processing stage alleviates much of the computational burden on the forward taps of a decision feedback equalizer (DFE) [7]. This allows the DFE to focus on channel inversion and minor phase tracking for the adaptive version.

The pre-processed complex data is then synchronized by using a cross-correlation match with initial training data and input to a fractionally-spaced equalizer. Section 5 evaluates five different equalizers. We found the inverse of the RMS error vector magnitude at the equalizer output to be related to the output SNR and observed bit error rates:

$$SNR \approx 20\log_{10}\left(\frac{1}{RMS\_error\_magnitude}\right) \tag{3}$$

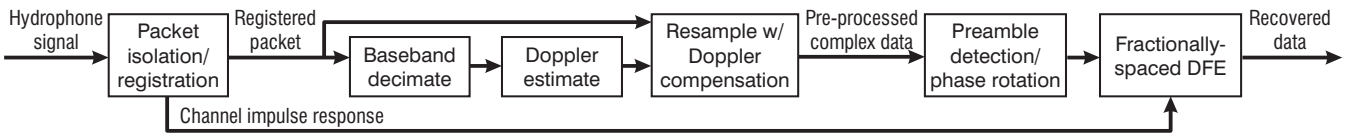

Fig. 7. Receiver block diagram.

Table 2. Design tradeoffs for three methods for estimating bulk Doppler shift, where M is the number of samples and c is the number of distinct frequencies to search over. In Method #2, accuracy increases with increasing c. Method #3 requires that a linear frequency modulated (LFM) sweep be added at the start of successive packets.

	Method	*Complexity*	*Accuracy*	*Constellations*
1	Fast Fourier transform	$M \log_2 M$	High	BPSK/QPSK
2	Cross-correlation	$M\,c$	Varies	Any
3	LFM sweeps	$M \log_2 M$	Low	Any

4. DOPPLER SHIFT ESTIMATION

We describe three methods for estimating the bulk Doppler shift, summarized in Table 2. Method #1 involves calculating the frequency of the near-DC component of a pre-emphasized version of the received data sequence by raising its M samples to the kth power where $k = 2$ for BPSK or $k = 4$ for QPSK and determining the dominant frequency of the resulting sequence. This method is not suitable for non-PSK modulations. Method #2 uses cross-correlation in the frequency domain to compare the received training sequence to a bank of replicas of the ideal training sequence waveform, where each replica has been contracted or expanded to simulate a particular Doppler shift. These encompass the expected range of shifts that can be encountered in environmental conditions.

Method #1 uses $O(M\log_2 M)$ operations and Method #2 requires $O(Mc)$ operations, where c is the number of replicas. When a wide range of detectable frequencies offsets is desired (e.g. involving hundreds of replicas), Method #2 is significantly more computationally expensive than Method #1, but is suitable for modulations that are of a higher order than QPSK. (Method #2 may be improved by techniques for reducing the replica bank search space).

Another approach, Method #3, is to estimate the average bulk Doppler shift by comparing the placement of LFM sweeps in successive packets to expected packet durations. This requires $O(M\log_2 M)$ operations. We found, however, that the frequency shift invariance of the sampled LFMs causes this approach to produce substandard results.

Theoretically, Doppler shift can also be detected by dynamic phase detection techniques as the high performance phase locked loop in [8]; such approaches can detect dynamic (e.g. non-bulk) changes throughout the duration of each packet. Because of problems often imposed by the channel's strong multipath, we instead opted to pair all adaptive phase detection functionality with the equalizer. Geller et al. in an earlier work in high-speed underwater communications employed similar rationale [9], and other works described in [1] locate PLL functionality in the equalizer rather than solely using adaptive DFE [10].

Table 3. Five fractionally-spaced equalizers considered for the equalization block in the receiver in Fig. 7. Many employ decision feedback equalization (DFE) and a least squares (LS) solution.

	Equalizer Description	*Forward*	*Feedback*
1	Single complex tap	1 tap	0 taps
2	Static DFE using an LS solution	L taps	N taps
3	Adaptive DFE initialized to LS solution	L taps	N taps
4	Multi-stage equalizer consisting of Equalizer #2 then single adaptive tap with high adaptation rate	L taps	N taps
5	Sparse DFE with taps located at symbols with largest impulse response magnitude	L taps	N taps

5. EQUALIZER COMPARISON

We evaluate the equalizer structures in Table 3 by describing the results seen in two Type 7 packets and two Type 5 packets. (See the waveform specifications in Table 1). These are representative of results seen in many other packets within our larger data set. Because of its higher accuracy and moderate computational complexity, *all data is bulk Doppler detected and corrected using Method #1.*

Equalizer #1 uses a single complex tap. Equalizer #2 is a static DFE whose L forward and N feedback taps are set to the least squares (LS) minimum mean squared error values for the training sequence. Equalizer #3 is an adaptive DFE that initializes to the LS solution and adapts at a rate of 0.1 of the upper stability limit $2 / N_{\text{total}}$ [10], where N_{total} is the total number of taps $L + N$. Equalizer #4 is a static DFE with a single forward tap and a high adaptation rate ($\mu = 0.1$). Equalizer #5 is a DFE with densely spaced forward taps. Similar to the heuristic tap placement approach in [11] and [9], Equalizer #5's sparsely spaced feedback taps are located at symbol intervals with highest channel impulse response magnitudes in a window of 0 ms (packet start) to 195 ms after the peak. The adaptation rate μ is $0 < \mu < 2 / N_{\text{total}}$. Other sparse equalization approaches not evaluated here include single-carrier frequency domain equalization [12] and various DFE methods for adaptive tap placement [1].

All equalizers use the same set of matrix operations to initialize the equalizer filter taps with the LS solution at each new packet. The complexity is $O(TN_{\text{total}}^2)$, where T is the training sequence length. (Equalizer #1's initialization is simplified, since $N_{\text{total}} = 1$.) All equalizers then perform the same series of operations with complexity $O(N_{\text{total}})$ per symbol in each packet. Here, each symbol is mapped to the receiver's decision space; the final data is then recovered.

Additional computations are performed in the adaptive Equalizers #3 and #4. The computation of error vectors and the adjustment of forward and feedback taps is $O(N_{\text{total}})$ per symbol for Equalizer #3, and $O(1)$ for Equalizer #4, as the latter operates with a single adaptive forward tap.

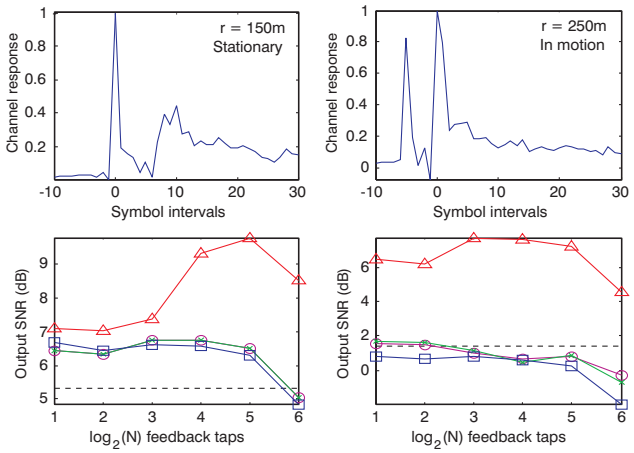

a. Type 7 Packet (BPSK, 1000 Hz symbol rate)

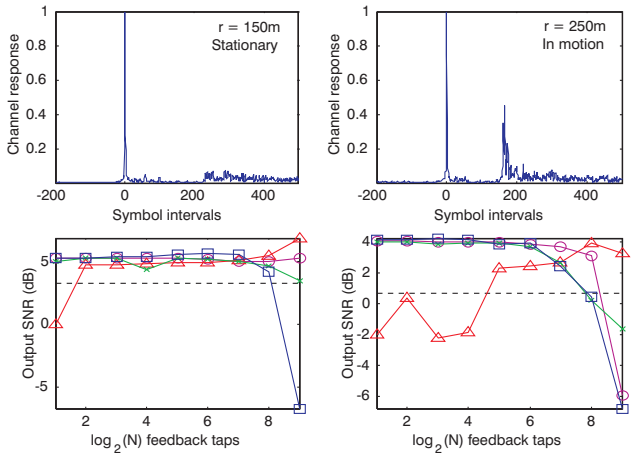

b. Type 5 Packet (QPSK, 32000 Hz symbol rate)

Legend: Equalizer #: -- 1, O 2, Δ 3, X 4, □ 5

Fig. 8. Performance of equalizers with 8 forward taps for a) Type 7 and b) Type 5 packets vs. number of feedback taps. Transmitter at range *r* is stationary (left column) or moving (right column). Refer to Table 3 for equalizer specifications.

Although these computational complexities reflect our current software-based receiver implementation, platform-specific improvements are readily possible and have been demonstrated. For example, matrix inversions may be performed through the modified squared Givens approach (a variant of QR decomposition) using fixed-point operations [13], and FIR filter operations may be pipelined [14].

For $L = 8$, Fig. 8 plots equalizer output SNR vs. $\log_2(N)$. The first 1000 and 100 symbols in Type 5 and 7 waveforms are used for training. For measured output SNR of 6 dB, bit error rates are 0.02 for QPSK and 0.002 for BPSK.

In Fig. 8a, the fully adaptive Equalizer #3 gives the highest output SNR in the Type 7 packets because it was able to track the channel over the packets' ~1 sec. duration. What the LS static structures learn in the training sequence changes significantly by the end of the packet.

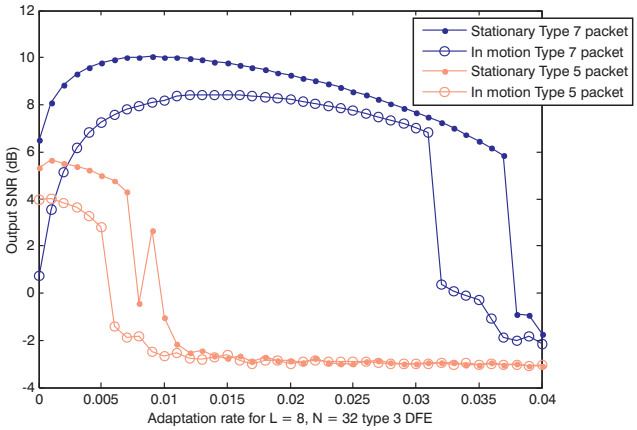

Fig. 9. Comparison of adaptation rates for an adaptive decision feedback equalizer (Equalizer #3 in Table 3) with 8 fwd. and 32 feedback taps for two types of packets and both types of mobility.

Table 4. Design tradeoffs for the five equalizer structures in Table 3. The output SNR is given for the best possible parameter settings.

Equalizer	*Training complexity*	*Packet Type 5 output SNR*	*Packet Type 7 output SNR*
1	Low	Low	Low
2	Medium	Medium	High
3	High	High	High
4	Medium	Medium	High
5	High	Medium	High

The output SNR of the Type 7 packets is impacted by the number of feedback taps used by the adaptive equalizer. In these results, the generally best performance is seen when $\log_2(N) = 5$. Performance declines when $\log_2(N) = 6$; the added taps cause the effective response rate to be reduced.

Fig. 8b (lower right pane) shows the effect of instability of the adaptive Equalizer #3 on the Type 5 packets when fewer feedback taps are used. A lower $\log_2(N)$ produces a higher adaptation rate, and the adaptive DFE makes so many incorrect decisions that it minimizes the mean squared error by centering itself in the middle of the constellation. It ignores all forward taps, bases its decision on previous decision(s) and outputs essentially random values. Such performance in a production system is highly undesirable.

Fig. 9 shows Equalizer #3 output SNR values for different adaptation rates. Differences in the optimal coefficient for the stationary and in-motion cases verify that the moving transmitter experiences a more rapidly varying channel. In the design of a production communication system, it is therefore appropriate to select an adaptation rate that corresponds with best output SNR values over an expected range of motion types and other environmental factors that are expected to be encountered.

Table 4 summarizes selected characteristics and design tradeoffs of each equalizer using the best parameter settings.

6. CONCLUSION

In this paper, we first characterize a shallow underwater acoustic communication channel using field measurements. We determine that the two dominant sources of distortion are Doppler shift and multipath propagation. In the measured channels, the channel impulse response is dozens of symbol periods long, and the multipath components contain at least half of the channel energy.

Then, the paper evaluates several design tradeoffs for a shallow underwater digital communication receiver. In the receiver, we first estimate the average frequency shift in each packet and then perform bulk Doppler shift correction. We evaluate three methods to estimate the average frequency shift, and find the best method to be raising the data to an even power and determing the dominant frequency.

After Doppler estimation and correction, we employ an equalizer for mitigating multipath. We evaluate five different equalizer structures, and find that the equalizer with adaptive feedforward and feedback taps gives the best communication performance. For the adaptive equalizer, we determine the best adaptation rate and best number of feedback taps for two measured channels.

We have collected 3 sets of field measurements on July 2009 (used for this paper), September 2009 [15], and November 2009 [16]. The November 2009 data set is available online [17].

ACKNOWLEDGEMENT

This research was supported by Independent Research and Development funds from the Applied Research Laboratories at The University of Texas at Austin in Austin, Texas.

REFERENCES

[1] D. B. Kilfoyle and A. B. Baggeroer, "The state of the art in underwater acoustic telemetry," *IEEE J. of Oceanic Eng.*, vol. 25, pp. 4–27, Jan. 2000.

[2] M. Chitre, S. Shahabudeen, and M. Stojanovic, "Underwater acoustic communications and networking: Recent advances and future challenges," *Marine Technology Society Journal*, vol. 42, pp. 103–116, Spring 2008.

[3] Texas Parks & Wildlife, "Lake Travis", 18 Jun 2009. http://www.tpwd.state.tx.us/fishboat/fish/recreational/lakes/travis/.

[4] Lower Colorado River Authority. "Historical Lake Levels: Lake Travis."
http://www.lcra.org/library/media/public/docs/histlvls/travis.xls.

[5] J. A. Catipovic, "Performance limitations in underwater acoustic telemetry", *IEEE J. of Oceanic Eng.*, vol. 15, no. 3, pp. 205-216, Jul. 1990.

[6] M. R. Ducoff and B. W. Tietjen, "Pulse Compression Radar", *Radar Handbook*, 3rd Ed., McGraw-Hill, pp. 8.3-8.11, 2008.

[7] M. Johnson, L. Freitag and M. Stojanovic, "Improved Doppler tracking and correction for underwater acoustic communications", in *Proc. IEEE Int. Conf. Acoustics, Speech and Sig. Proc.*, vol. 1, pp. 575-578, 1997.

[8] V. Torres, A. Perez-Pscual, A. T. Sansaloni, J. Valls, "Design of high performance timing recovery loops for communication applications", *Proc. IEEE Workshop on Signal Processing Systems*, pp. 1-4, 2006.

[9] B. Geller, V. Capellano, G. Jourdain, "Equalizer for real time high rate transmission in underwater communications", *Proc. IEEE Int. Conf. Acoustics, Speech, and Signal Processing*, vol. 5, pp. 3179-3182, 1995.

[10] D. G. Messerschmitt and E. A. Lee, *Digital Communication*, Kluwer Academic Press, 1988.

[11] A. Chopra and B. L. Evans, "Design of sparse filters for channel shortening", *Proc. IEEE Int. Conf. on Acoustics, Speech, and Signal Proc.*, Mar. 14-19, 2010.

[12] R. A. Iltis, "Iterative joint decoding and sparse channel estimation for single-carrier modulation", *Proc. IEEE Int. Conf. Acoustics, Speech and Signal Processing*, pp. 2689-2692, 2008.

[13] L. Ma, K. Dickson, J. McAllister, J. McCanny, M. Sellathurai, "Reduced-complexity MSGR-based matrix inversion", *Proc. IEEE Workshop on Signal Processing Systems*, pp.124-128, 2008.

[14] Y. Lai, C. Kao, H. Chen, "Design and implementation of an adaptive FIR filter based on delayed error LMS algorithm", *Proc. IEEE Workshop on Signal Processing Systems*, pp. 704-712, 1999.

[15] K. Nieman, K. Perrine, T. Henderson, K. Lent, T. Brudner, B. Evans, "Wideband monopulse spatial filtering for large array receivers for reverberant underwater communication channels", *Proc. IEEE OCEANS*, 2010.

[16] K. Perrine, K. Nieman, T. Henderson, K. Lent, T. Brudner, B. Evans, "Doppler estimation and correction for shallow underwater acoustic communications", *Proc. 43nd Asilomar Conference on Signals, Systems and Computers*, 2010.

[17] K. Perrine, K. Nieman, K. Lent, T. Henderson, T. Brudner, B. Evans, "The University of Texas at Austin Applied Research Laboratories Nov. 2009 five-element acoustic underwater dataset," 30 June 2010.
http://users.ece.utexas.edu/~bevans/projects/underwater/datasets/index.html.